Laser and Particle Beams (2014), *32*, 375–381.

doi:10.1017/S026303461400024X

Effects of transverse static electric field on terahertz radiation generation by beating of two transversely modulated Gaussian laser beams in a plasma

PRATEEK VARSHNETY, VIVEK SAJAL, PRASHANT CHAUHAN, RAVINDRA KUMAR, AND NAVNEET K. SHARMA

Department of Physics and Material Science and Engineering, Jaypee Institute of Information Technology, Uttar Pradesh, India

(RECEIVED 24 January 2014; ACCEPTED 22 April 2014)

Abstract

Resonant excitation of terahertz (THz) radiation by nonlinear coupling of two filamented spatial-Gaussian laser beams of different frequencies and wave numbers is studied in plasma having transverse static electric field. The static ponderomotive force due to filamented lasers is balanced by the pressure gradient force which gives rise to transverse density ripple, while, the nonlinear ponderomotive force at frequency difference of beating lasers couples with density ripple giving rise to stronger transverse nonlinear current which results into the excitation of THz radiation at resonance. The coupling is further enhanced by the presence of static electric field and spatial-Gaussian nature of laser beams. An increase of six-fold in the normalized amplitude of THz is observed by applying a direct current field of about 50 KV. Effects of frequency, laser beam width, and periodicity factor of modulated laser amplitude are studied for the efficient THz radiation generation. These results can be utilized for generating controlled tunable THz sources for medical applications using low filament intensities ($\sim 10^{14}$ W/cm^2) of beating lasers.

Keywords: Gaussian laser; Magnetized plasma; Terahertz generation

1. INTRODUCTION

In last few years, Terahertz (THz) radiation generation (Dua *et al*., 2011; Hu *et al*., 2010; Sharma *et al*., 2010; Varshney *et al*., 2013) has attracted a lot of interest due to its potential applications in material characterization, imaging, topography, remote sensing, chemical and security identification, explosive detection, outer space communication, etc. (Ferguson *et al*., 2002; Shen *et al*., 2005; Zheng *et al*., 2006; Pickwell *et al*., 2006; Antonsen *et al*., 2007; Liu *et al*., 2009; Malik *et al*., 2010). Conventional methods employing electro-optic crystals and semiconductors are not efficient enough to achieve high energy pulses of THz radiation (Faure *et al*., 2004; Shi *et al*., 2002; Zhao *et al*., 2010) due to their lower damage limit. To achieve this objective, plasma is utilized as a nonlinear medium in various schemes (Kumar *et al*., 2013; Giulietti *et al*., 1988; Panwar *et al*., 2013; Garg *et al*., 2010; Ghorbanalilu *et al*., 2012; Verma *et al*., 2009) employing a strong laser plasma interaction (Verma *et al*., 2011; Paknezhad *et al*., 2011) because plasma can handle very high power lasers and it has an added advantage of not having damage limit (Jiang *et al*., 2011; Leemans *et al*., 2004; Pukhov *et al*., 2003; Hashimshony *et al*., 1999; Tani *et al*., 2000; Loffler *et al*., 2005; Breunig *et al*., 2008). Out of various schemes proposed in the literature, THz pulse energy achieved from laser filaments is quite high (Wang *et al*., 2011; Ladouceur *et al*., 2001; Tripathi *et al*., 1990; Loffler *et al*., 2000; Houard *et al*., 2008) as compared to other schemes like coherent radiation from plasma oscillations driven by ultra-short laser pulses (Hamster *et al*., 1993; 1994), synchrotron radiation from accelerated electrons (Carr *et al*., 2002), the transition radiation of electron beams (Abo-Bakar *et al*., 2003), etc. Wang *et al*. (2011) have experimentally observed 570 nJ THz pulse energy at frequency ≤5.5 THz, at a distance of ∼ 10 m by two color femtosecond filamentation in air.

Ladouceur *et al*. (2001) were among the first to observe broadband THz radiation employing the plasma filaments (electron density $\sim 10^{16}$ m^{-3} at 0.9 THz plasma frequency) formed through multi-photon ionization by a 100 fs laser

Address correspondence and reprint requests to: Vivek Sajal, Department of Physics and Material Science & Engineering, Jaypee Institute of Information Technology, Noida-201307, Uttar Pradesh, India. E-mail: vsajal@rediffmail.com

pulse propagating in air and achieved power conversion efficiency of $\sim 10^{-9}$. Tripathi *et al.* (1990) investigated THz radiation generation in air via bi-filamentation of two co-propagating femtosecond laser pulses with suitable time delay. For a time delay of less than 2 ns, the amplitude of 0.1 THz frequency radiation was found to be 10 times higher than the one due to a single pulse. However, for other frequencies, it could be greater or less than 10. When a femtosecond laser pulse propagates through air, it undergoes filamentation and self-focusing and forms the plasma channel which, attains strong dipole moment and emits electromagnetic radiation. The radiation frequency can be controlled and maintained in the THz range by choosing suitable plasma parameters.

Loffler *et al.* (2000) reported a large enhancement of intensity of THz radiation emitted by ionized air in the presence of a static electric field. They observed a current surge following photo-ionization of the air with an applied bias field of 10.6 KV/cm leading to the emission of THz pulses with an intensity which can be almost as high as that of THz pulses radiated from a large-area intrinsic-field GaAs emitter. Recently, Houard *et al.* (2008) observed a three order of magnitude of enhancement of the THz energy radiated by a femtosecond pulse undergoing filamentation in air in the presence of static electric field. The emitted THz wave was found to be linearly polarized in the plane containing the static electric field. They also provided a theoretical model which predicts that the total emitted energy is proportional to the square of the filament cross-section, square of direct current (dc) electric field, filament length, and plasma density in the channel in the power 3/2. Bhasin *et al.* (2011) also studied the THz radiation generation from laser filament in the presence of a static electric field in plasma. They observed an enhancement in coupling in the presence of the static electric field. The ratio of THz amplitude to that of filament amplitude is the order of 10^{-5} at laser intensities $\sim 10^{14}$ W/cm^2.

The THz amplitude obtained by the scheme proposed by Bhasin *et al.* (2011) can be improved many times by considering more realistic Gaussian profile of laser filaments. In the present work, we have studied the combined effects of Gaussian profile, static electric field, and filamented nature of lasers on THz radiation generation by beating of two co-propagating laser beams in plasma (Fig. 1). Transverse amplitude modulated lasers exert not only a nonlinear ponderomotive force $F_{p\omega}$ at beat frequency (ω) but a space periodic ponderomotive force F_{pq}, which in association with gradient force produces transverse density ripples (of zero frequency and wave number $\vec{q}$) in the plasma. Plasma electrons, oscillated under the influence of beat frequency ponderomotive force give rise to density perturbation at frequency ω and wave number $\vec{k}$ as well as $\vec{k}+\vec{q}$. Density perturbations couple with drift velocity ($\vec{v}_{dc}$) due to static electric field in rippled plasma and produce a nonlinear current at frequency ω and wave number $\vec{k}+\vec{q}$ which is responsible for THz radiation generation at resonance. In Section 2,

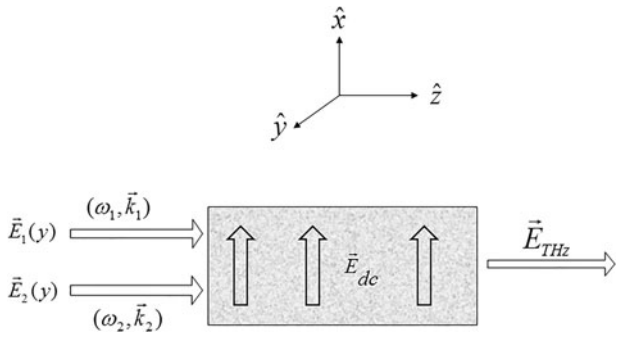

Fig. 1. Schematic diagram of beat excitation of THz radiation in the presence of transverse static electric field $\vec{E}_{dc}$.

expressions for the ponderomotive force, density perturbation, and nonlinear current responsible for THz generation are derived and the wave equation for THz wave is solved to calculate its amplitude. Conclusions are given in Section 3.

2. THZ RADIATION GENERATION DUE TO LASER BEATING

Consider two transversely modulated Gaussian laser beams co-propagating through the pre-existing plasma having electron plasma density n_0^0. The field profile of lasers is given by

$$\vec{E}_j = \hat{y}[1+\mu_j \cos qy]E_{j0}e^{-(\omega_j t - k_j z)} \qquad j = 1, 2. \tag{1}$$

where $E_{j0} = A_{j0}e^{-y^2/a_0^2}$; μ_j is the index of modulation, a_0 is the beam width, and q is the periodicity parameter. Dispersion relation of beating lasers is $k_j^2 = (\omega_j^2/c^2)\{1-(\omega_p^2/\omega_j^2)\}$. The frequency difference of the lasers $\omega = \omega_1 - \omega_2$ lies in the THz range. The laser filaments impart oscillatory velocities to plasma electrons, given by

$$\vec{v}_j = \frac{e\vec{E}_{j0}}{mi\omega_j}. \tag{2}$$

The plasma is embedded with a dc electric field $\vec{E}_{dc} \| \hat{x}$ which provides dc velocity component to plasma electrons

$$\vec{v}_{dc} = -\frac{e\vec{E}_{dc}}{m\nu_e} \tag{3}$$

where $-e$, m, and ν_e are the charge, mass, and collision frequency of plasma electrons. Here, Debye shielding related aspects can be considered by assuming that plasma is formed by focusing Ti:Sa CPA (chirped pulse amplified) laser beam on hydrogen gas or air (Houard *et al.*, 2008). The created plasma filament is modeled by specific electric field profile of beating laser given by Eq. (1). When external static electric field $\vec{E}_{dc}$ is applied across the plasma filament by placing two copper plane electrodes, plasma electrons start moving under the influence of the field. The charge is accumulated at the edge of filament and electric field is completely screened in

https://doi.org/10.1017/S026303461400024X Published online by Cambridge University Press

the plasma. However, there is a transient process of redistribution of charges, and the temporal behavior of the electric current depends on relation between three parameters: the duration of the ionization process t_{ion}, the electron collision time t_{col} and the period of plasma oscillations. For typical laser pulse duration of 50 fs, the electron plasma density will be $\sim 10^{16}$ cm^{-3} in a filament of radii 30–50 μm. Then, plasma period is approximately 1 ps, the collision time is ~100 ps; both of them longer than ionization time. Therefore one can consider the response of plasma with an instantaneous ionization, and the electric current which is directed along the direction of the external electric field (Houard *et al.*, 2008).

Beating picosecond CO_2 lasers are launched in the pre-existing plasma embedded with static field. Their pulse duration is greater than plasma period (~1 ps) so use of monochromatic wave approximation is justified in the present scheme. Lasers beat together in presence of static electric field and exert a ponderomotive force F_p on plasma electrons given by

$$\vec{F}_p = \vec{F}_{pq} + \vec{F}_{p\omega}, \tag{4}$$

where $\vec{F}_{pq}$ is static ponderomotive force, given by

$$\begin{aligned} F_{pq} = {} & \frac{e^2 A_1^2}{2m\omega_1^2}\left[\nabla + \hat{y}\left\{\frac{-2y}{a_0^2} - \frac{\mu_1 q \sin qy}{1+\mu_1 \cos qy}\right\}\right] \\ & \times \left[1+\mu_1 \cos qy\right]^2 e^{-2y^2/a_0^2} \\ & + \frac{e^2 A_2^2}{2m\omega_2^2}\left[\nabla + \hat{y}\left\{\frac{-2y}{a_0^2} - \frac{\mu_2 q \sin qy}{1+\mu_2 \cos qy}\right\}\right] \\ & \times \left[1+\mu_2 \cos qy\right]^2 e^{-2y^2/a_0^2} \end{aligned} \tag{4a}$$

By substituting $\cos qy = (e^{iqy} + e^{-iqy})\ /\ 2$ and $\sin qy = (e^{iqy} + e^{-iqy})/2i$, Eq. (4a) can be simplified to give an expression having two term e^{iqy} and e^{-iqy}. Out of these two, term having e^{iqy} is responsible for exciting THz radiation at resonance condition. Term having e^{-iqy} will be off resonant and can be neglected.

$$\vec{F}_{pq} = \frac{e^2}{4m}\left[\nabla\hat{z} + \left(-\frac{2y}{a_0^2}\right)\hat{y}\right]\left[\frac{\mu_1 A_{01}^2}{\omega_1^2} + \frac{\mu_2 A_{02}^2}{\omega_2^2}\right] e^{iqy} e^{-2y^2/a_0^2}, \tag{4b}$$

$\vec{F}_{p\omega}$ is beat frequency ponderomotive force at frequency $\omega = \omega_1 - \omega_2$, given by

$$\vec{F}_{p\omega} = \frac{e^2}{2m\omega_1\omega_2}\left[\vec{\nabla} + \hat{y}\left\{\frac{4y}{a_0^2} + q\left(\frac{\mu_1+\mu_2}{2}\right)e^{iqy}\right\}\right]\vec{E}_1 \cdot \vec{E}_2^*. \tag{5}$$

The static ponderomotive force causes ambipolar diffusion of plasma along $\hat{y}$. In the present study, time scale of diffusion is ~12 ps at 5 eV electron plasma temperature, which is much larger than the pulse duration (Malik *et al.*, 2013). In the steady state, the static ponderomotive force is balanced by the pressure gradient force giving rise to zero frequency transverse density ripple (Bhasin *et al.*, 2011),

$$n_{0q} = \frac{1}{2}\frac{n_0^0}{T_e}\frac{e^2}{4m}\left[\frac{\mu_1 A_{01}^2}{\omega_1^2} + \frac{\mu_2 A_{02}^2}{\omega_2^2}\right] e^{iqy} e^{-2y^2/a_0^2}, \tag{6}$$

where T_e is the equilibrium electron temperature. The beat frequency ponderomotive force imparts nonlinear oscillatory velocity $\vec{v}_\omega^{NL}$ to plasma electrons, which is evaluated by using the equation of motion. The nonlinear velocity at frequency $\omega = \omega_1 - \omega_2$ has following two components at wave number $\vec{k} = \vec{k}_1 - \vec{k}_2$ and $\vec{k} + q$

$$v_{\omega,\vec{k}}^{NL} = \frac{e^2 A_{01} A_{02}^* k}{2m^2\omega\omega_1\omega_2} e^{-2y^2/a_0^2} e^{-i(\omega t - kz)}\hat{z}, \tag{7}$$

$$v_{\omega,\vec{k}+\vec{q}}^{NL} = \frac{e^2 A_{01} A_{02}^* (\mu_1+\mu_2)}{4m^2\omega\omega_1\omega_2}\left[2q\hat{y} + k\hat{z}\right] e^{-2y^2/a_0^2} e^{-i(\omega t - kz - qy)}. \tag{8}$$

The density perturbations $\vec{n}_{\omega,\vec{k}}^{NL}$ and $\vec{n}_{\omega,\vec{k}-\vec{q}}^{NL}$ caused by the velocity perturbation (given by Eqs. (7)–(8)) are calculated by solving continuity equation

$$\vec{n}_{\omega,\vec{k}}^{NL} = \frac{e^2 A_{01} A_{02}^* n_0^0 k^2}{2m^2\omega^2\omega_1\omega_2} e^{-2y^2/a_0^2} e^{-i(\omega t - kz)}, \tag{9}$$

$$\begin{aligned} \vec{n}_{\omega,\vec{k}+\vec{q}}^{NL} = {} & \frac{e^2 A_{01} A_{02}^* (\mu_1+\mu_2) k^2}{4m^2\omega\omega_1\omega_2} e^{-2y^2/a_0^2} e^{-i(\omega t - kz - qy)} \\ & + \frac{e^2 A_{01} A_{02}^* (\mu_1+\mu_2) 2q^2}{4m^2\omega\omega_1\omega_2} e^{-2y^2/a_0^2} e^{-i(\omega t - kz - qy)} \\ & + \frac{e^2 A_{01} A_{02}^* (\mu_1+\mu_2)}{4m^2\omega\omega_1\omega_2}\frac{8qy}{a_0^2} e^{-2y^2/a_0^2} e^{-i(\omega t - kz - qy - \pi/2)} \end{aligned} \tag{10}$$

Eqs. (7)–(8) can be easily reduced to expression obtained by Bhasin *et al.* (2011) by assuming planer wave front in place of Gaussian profiles of beating lasers. Following Bhasin *et al.* (2011), one may write the nonlinear current density at $(\omega, \vec{k})$ as:

$$\begin{aligned} \vec{J}_{\omega,\vec{k}}^{NL} &= \vec{J}_1 + \vec{J}_2 + \vec{J}_3 \\ \vec{J}_{\omega,\vec{k}}^{NL} &= -n_0^0 e\vec{v}_{\omega,\vec{k}}^{NL} - \vec{n}_{\omega,\vec{k}}^{NL} e\vec{v}_{dc} - n_{0q}^* e\vec{v}_{\omega,\vec{k}+\vec{q}}^{NL} \end{aligned} \tag{11}$$

Here, the first term arises due to the coupling between equilibrium plasma densities n_0^0 and nonlinear velocity $\vec{v}_{\omega,\vec{k}}^{NL}$, the second term is due to nonlinear coupling between nonlinear density perturbation $\vec{n}_{\omega,\vec{k}}^{NL}$ and dc electron velocity $\vec{v}_{dc}$, and the third term is the result of coupling between zero frequency transverse density ripple $n_{0q}{}^*$ and nonlinear velocity $\vec{v}_{\omega,\vec{k}+\vec{q}}^{NL}$. The dc electric field changes the THz radiation generation scenario due to the coupling between nonlinear density perturbation $\vec{n}_{\omega,\vec{k}}^{NL}$ and large dc velocity of plasma electrons in presence of dc electric field (Loffler *et al.*, 2000; Bhasin

https://doi.org/10.1017/S026303461400024X Published online by Cambridge University Press

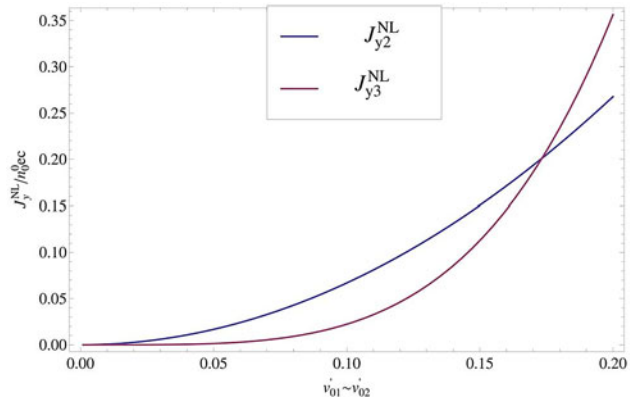

Fig. 2. (Color online) Plot of normalized current density $J_y^{NL} / n_0^0 ec$ as a function of normalized electron velocity v_{01}'. Other parameters are q'=0.3, $k' \approx 0.01$, $\mu_1 \sim \mu_1 \sim 0.3$, $\omega_1' = 50$, $v_{dc}' = 0.053$, $\omega' = 3$ and $y/a_0 = 0.1$.

et al., 2011). Due to large electron collision time period ~100 ps, plasma electron achieves large drift velocity ($v_{dc} = -eE_{dc}/m\upsilon_e$) in presence of applied dc electric field. As a result of which nonlinear current contribution due to J_2 becomes significant as compared to J_3 (for lower values of pump intensities), as shown in Figure 2. Resolving Eq. (11) into y and z components, we obtain

$$J_{y\omega,k}^{NL} = \frac{n_0^0 e^4 A_{01} A_{02}^*}{2m^3 \omega \omega_1 \omega_2} \left[\frac{k^2 E_{dc}}{\nu_e \omega} - \frac{eq(\mu_1+\mu_2)}{8T_e}\left\{\frac{\mu_1 A_{01}^2}{\omega_1^2} + \frac{\mu_2 A_{02}^2}{\omega_2^2}\right\} e^{-2y^2/a_0^2}\right] e^{-2y^2/a_0^2} e^{-i(\omega t - kz)}, \tag{12a}$$

$$J_{z\omega,k}^{NL} = -\frac{n_0^0 e^3 A_{01} A_{02}^* k}{2m^2 \omega \omega_1 \omega_2} \left[1 + \frac{e^2(\mu_1+\mu_2)}{16mT_e}\left\{\frac{\mu_1 A_{01}^2}{\omega_1^2} + \frac{\mu_2 A_{02}^2}{\omega_2^2}\right\} e^{-2y^2/a_0^2}\right] e^{-2y^2/a_0^2} e^{-i(\omega t - kz)}. \tag{12b}$$

It can be observed from Eq. (12) that J^{NL} varies as $\sim e^{-i(\omega t - kz)}$, where $\vec{k} = \vec{k}_1 - \vec{k}_2 + \vec{q}$, and it is responsible for THz radiation generation. It is clear that wave number q of electrostatic density ripples is responsible for providing extra momentum to achieve resonance condition. The periodic nature of transverse density ripples is must, otherwise, $\vec{k}(= \vec{k}_1 - \vec{k}_2 + \vec{q})$ will exhibit non-periodic behavior; resonance condition cannot be achieved and maximum energy transfer will not take place and consequently a weak field THz radiation will be generated (Varshney *et al.*, 2013). The transverse y-component of wave equation governing the propagation of THz wave can be written as

$$\frac{\partial^2 E_y}{\partial z^2} + \left(\frac{\omega^2 \varepsilon}{c^2}\right) E_y = \frac{-4\pi i \omega}{c^2} \vec{J}_y^{NL}, \tag{13}$$

where, $\varepsilon(\omega) = 1 - \omega_p^2 / \omega^2$ is the plasma permittivity at the THz frequency and $\omega_p^2 = 4\pi n_0^0 e^2 / m$. The dispersion relation of THz wave is given by $k^2 = (\omega^2/c^2)(1 - \omega_p^2/\omega^2)$ which is obtained by placing the right-hand side of Eq. (13) (i.e., source term) equal to zero. This mode can freely propagate through the plasma if $\omega > \omega_p$. This can also be observed from the plot between normalized propagation vector (kc/ω_p) and normalized frequency (ω/ω_p) of THz radiation in Figure 3. To plot this figure, we have utilized resonance conditions $\omega = \omega_1 - \omega_2$ and $\vec{k} = \vec{k}_1 - \vec{k}_2 + \vec{q}$. In this study, $\omega/\omega_p = 2.5 - 5$ (corresponding to 8 THz to 30 THz), which satisfy the above said condition ($\omega > \omega_p$). Thus, this mode can easily propagate through the plasma. Field profiles of co-propagating lasers given by Eq. (1) also satisfy the dispersion relation $k^2 = (\omega^2/c^2)(1 - \omega_p^2/\omega^2)$. For the present set of parameters plasma frequency $f_p \approx 100\ \nu_p$, where ν_p is the collision frequency. Thus, use of collisionless plasma dispersion relation is justified. Eq. (13) can be solved over the length L of the plasma column and the normalized THz amplitude can be written as follows:

$$A_y = \left|\frac{E_y}{A_{01}}\right| \approx \frac{v_{02}' q'}{16}\left[\mu_1 v_{01}'^2 + \mu_2 v_{02}'^2\right] \frac{\mu_1+\mu_2}{\sqrt{\varepsilon}(\sqrt{\varepsilon}-1)\omega_1' k'^2} e^{-2y^2/a_0^2} + \frac{v_{02}' v_{dc}'}{2\omega_1' \omega' \sqrt{\varepsilon}(\sqrt{\varepsilon}-1)} e^{-2y^2/a_0^2} \tag{14}$$

where $v_{01}' = eA_{01} / m\omega_1 c$, $v_{02}' = eA_{02} / m\omega_2 c$, $v_{dc}' = eE_{dc} / m\nu_e c$, $q' = qc / \omega_p$, $k' = k\nu_{th} / \omega_p$, $\omega_1' = \omega_1 / \omega_p$, and $\omega_2' = \omega_2 / \omega_p$. Eq. (14) does not depend on the plasma length because we are concerned only with stationary solutions for THz radiation generation. The THz radiation can easily propagate out of the plasma because damping for THz electromagnetic wave is negligible for the parameters of present scheme and even plasma length can be adjusted in experimental set-ups according to the skin depth of plasma. One can notice that normalized THz amplitude is directly proportional to laser power, but dc electric field term (second term) is very small as compared to beat wave ponderomotive force term (first term) at high filament intensities in Eq. (14). To check the contribution of the two terms on the right-hand

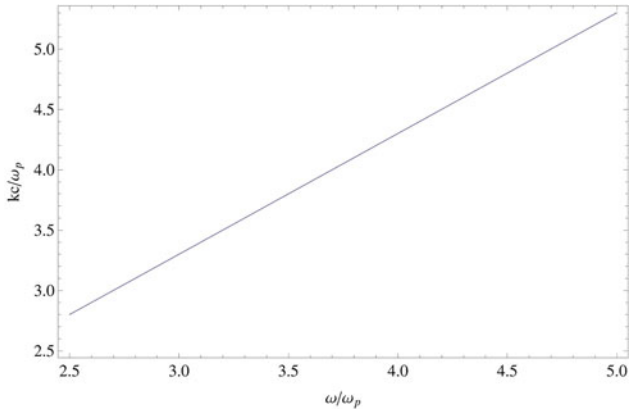

Fig. 3. (Color online) Plot of dispersion relation of THz radiation.

https://doi.org/10.1017/S026303461400024X Published online by Cambridge University Press

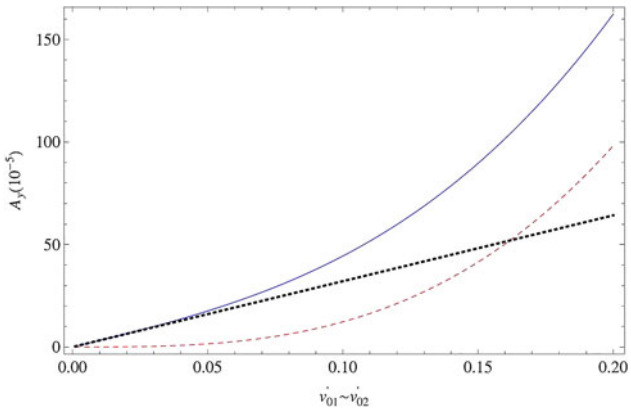

Fig. 4. (Color online) Plot of normalized THz amplitude as a function of normalized electron velocity $v'_{01} \sim v'_{02}$ by (**i**) considering only first term of Eq. (14) on right-hand side (dashed line), (**ii**) considering only second term of Eq. (14) on right-hand side (dotted line), and (**iii**) considering both terms of Eq. (14) on RHS (solid line). Other parameters are $q' = 0.3$, $k' \approx 0.01$, $\mu_1 \sim \mu_1 \sim 0.3$, $\omega'_1 = 50$, $v'_{dc} = 0.053$, $\omega' = 3$ and $y/a_0 = 0.1$.

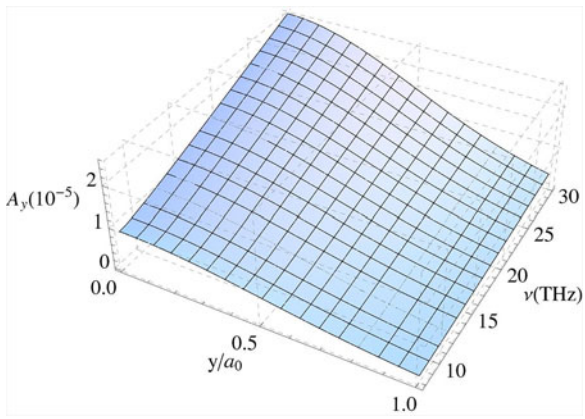

Fig. 5. (Color online) Variation of normalized THz amplitude as a function of THz frequency υ and normalized beam width parameter y/a_0. Other parameters are $q' = 0.3$, $k' \approx 0.01$, $\mu_1 \sim \mu_1 \sim 0.3$, $\omega'_1 = 50$, $v'_{dc} = 0.053$ and $v'_{01} \sim v_{02}{}' \sim 0.005$.

side of Eq. (14), we plot the variation of normalized amplitude of THz wave with respect to normalized oscillatory velocities $v'_{01} \sim v'_{02}$ of beating laser in Figure 4. In the present work, there are two types of ponderomotive forces due to lasers envelop: (1) Static ponderomotive force $\vec{F}_{pq}$ which does not contribute directly in exciting THz generation, but forms transverse density ripples by balancing the pressure gradient force. These density ripples provides necessary mismatch in $\vec{k}$ values at resonance. (2) Beat frequency ponderomotive force $\vec{F}_{p\omega}$ at frequency $\omega = \omega_1 - \omega_2$. $\vec{F}_{p\omega}$ is directly responsible for enhancing the amplitude of THz radiation.

Another force responsible for enhancing the amplitude of THz radiation is electric force due to applied dc electric field $\vec{E}_{dc}$. Thus $\vec{F}_{p\omega}$ and $-e\vec{E}_{dc}$ forces on plasma electrons contribute directly to THz amplitude. First and second term on the right-hand side of Eq. (14) represent contribution of $\vec{F}_{p\omega}$ and $-e\vec{E}_{dc}$ forces to the amplitude A_y of the THz radiation, respectively. Their relative contributions are observed by plotting both the terms as a function of v'_{01} ($\sim v'_{02}$) in Figure 4. Up to $v'_{01} \cong 0.16$ electric force contribution is more effective ($|-e\vec{E}_{dc}| > \vec{F}_{p\omega}$), while after $v'_{01} > 0.16$ contribution of $\overleftarrow{F}_{p\omega}$ becomes more significant than $-e\vec{E}_{dc}$ force ($\vec{F}_{p\omega} > |-e\vec{E}_{dc}|$). Intensities of beating lasers [$I = (1.384 \times 10^{18})(a_0^2 / \lambda^2)$, here I is in W/cm^2, λ in micron] come out to be $\sim 10^{14}$ W/cm^2 corresponding to $v'_{01} \approx v'_{01} \approx 0.16$. $\lambda = 10$ μm are chosen corresponding to picosecond CO_2 laser. Thus, effects of dc electric field can be utilized only at low filament intensities ($\sim 10^{14}$ W/cm^2) of beating lasers. Eq. (14) reveals that the normalized THz amplitude is proportional to square of filament cross-section (μ_1^2, μ_2^2 and $\mu_1\mu_2$), thus, THz field increases on increasing μ_1 and μ_2. Its explanation lies in Eqs. (6) and (12); higher the value of μ_1 and μ_2, greater the amplitude of density ripples n_{q0} (Eq. (6)) which means, higher number of electrons will be involved in the generation of oscillatory nonlinear current $\vec{J}^{NL}_{\omega,k}$ (Eq. (12)). Higher number of charge carriers result into higher nonlinear current which leads to more efficient THz radiation. In Figure 5, variation of normalized THz amplitude is shown as a function of THz frequency (v) and beam width parameter (y/a_0) at $v'_{01} \sim v'_{02} \sim 0.005$. THz amplitude increases with THz frequency. The increase in THz amplitude can be attributed to the change in plasma permittivity $\varepsilon(\omega) = 1 - \omega_p^2 / \omega^2$ as a function of THz frequency (ω). The factor ($\sqrt{\varepsilon} - 1$) appearing in the denominator of Eq. (14) decreases 2.5 times as ω/ω_p changes from 2.5 to 5, which results into approximately two-fold increases in THz amplitude. THz amplitude is maximum at axis ($y/a_0 = 0$) and decreases as one moves off axis. In Figure 6, we plot normalized THz amplitude as a function dc electric field E_{dc}(KV/cm) and beam width parameter (y/a_0) for following set of parameters: $q' = 0.3$, $k' \approx 0.01$, $\mu_1 \sim \mu_1 \sim 0.3$, $\omega'_1 = 50$, $\omega' = 3$ and $y/a_0 = 0.1$. It is observed that as one increases E_{dc}, normalized THz amplitude increases continuously at normalized velocity $v'_{01} \sim v'_{02} \sim 0.005$. THz amplitude is nearly two times higher as compared to the

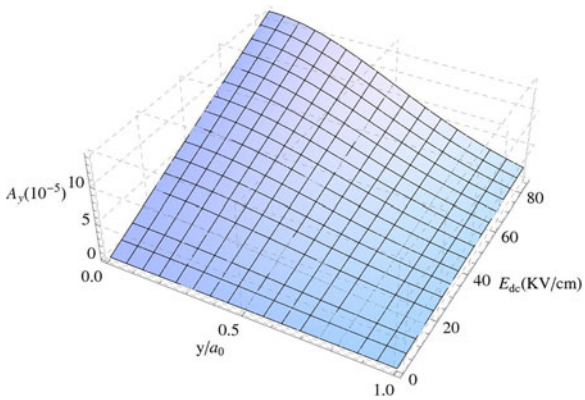

Fig. 6. (Color online) Plot of normalized THz amplitude as a function of dc electric field E_{dc} and normalized beam width parameter y/a_0. Other parameters are $q' = 0.3$, $k' \approx 0.01$, $\mu_1 \sim \mu_1 \sim 0.3$, $\omega'_1 = 50$, $\omega' = 3$ and $v'_{01} \sim v'_{02} \sim 0.005$.

https://doi.org/10.1017/S026303461400024X Published online by Cambridge University Press

scheme suggested by Bhasin *et al.* (2011), for the same set of parameters. Effects of finite laser spot size are not included in the present scheme because the maximum off axis distance utilized in the present scheme is up to $y/a_0 = 1$. In the present scheme plasma is considered unmagnetized where polarization field effect are not significant (Chen *et al.*, 1983).

3. CONCLUSIONS

We have studied the dynamics of generation of THz wave by the beating of two laser beams in the presence of static electric field, when only ponderomotive nonlinearity is operative. Gaussian envelop of filamented laser beams is considered in the scheme. The nonlinear mechanism which generates the THz radiation can be understood as follows: the nonlinear interaction of the laser beams with the plasma having static magnetic field generates the velocity perturbation which leads to density perturbation in the electron density. Static electric field also imparts dc velocity to electrons. Two components of ponderomotive force (Eqs. (4) and (5)) are responsible for density perturbation. As a result, a nonlinear current at beat wave frequency is generated due to the coupling between various density and velocity components of electrons as shown in Eq. (12). Since the difference in laser beam frequencies is in the range of THz and phase matching conditions are satisfied, the nonlinear current generated at beat frequency generates the desired THz wave. The THz amplitude can be controlled by laser-plasma parameters and magnitude of static electric field as shown in Eq. (14). Taking into account the Gaussian envelop, the growth of THz radiation amplitude is increased almost 10 times when the magnitude of normalized oscillatory velocities is increased from 0.005 to 0.01 in comparison to plane laser beams suggested by Bhasin *et al.* (2011). THz amplitude also increases significantly with the beat wave frequency. Our numerical results also show that amplitude of THz is high at small y/a_0, which shows that laser plasma interaction in paraxial region may play an important role to enhance the amplitude of THz. All these results can be useful in developing THz pulsed imaging as a medical imaging tool because the THz amplitude can be easily tuned by changing applied dc electric field upto the intensity level of $\sim 10^{14}$ W/cm^2. The THz frequencies correspond to energy levels of molecular rotations and vibrations of DNA (Markelz *et al.*, 2000) and proteins (Walther *et al.*, 2000), which may provide characteristic fingerprints to differentiate biological tissues in a region of the spectrum not previously explored for medical use. THz wavelengths are particularly sensitive to water and exhibit absorption peaks due to stretching modes at 6 THz and vibrational modes at 19.5 THz. This makes the technique very sensitive to hydration state (Mittleman *et al.*, 1996) which can indicate tissue condition.

REFERENCES

Abo-Bakr, M., Feikes, J., Holldack, K., Kuske, P., Peatman, W.B., Schade, U., Wustefeld, G. & Hübers, H.W. (2003). Brilliant, coherent far-infrared (THz) synchrotron radiation. *Phys. Rev. Lett.* **90**, 094801.

Antonsen, T.M., Palastra, J.J. & Milchberg, H.M. (2007). Excitation of terahertz radiation by laser pulses in nonuniform plasma channels. *Phys. Plasmas* **14**, 033107.

Bhasin, L. & Tripathi, V.K. (2011). Terahertz generation from laser filaments in the presence of a static electric field in a plasma. *Phys. Plasma* **18**, 123106.

Breunig, I., Kiessling, J., Sowade, R., Knabe, R. & Buse, K. (2008). Generation of tunable continuous-wave terahertz radiation by photo mixing the signal waves of a dual-crystal optical parametric oscillator. *New J.Phys.* **10**, 073003.

Chen, F.F. (1983). *Introduction to Plasma Physics and Controlled Fusion*. New York: Plenum Press.

Carr, G.L., Martin, M.C., Mckinney, W.R., Jordan, K., Neil, G.R. & Williams, G.P. (2002). High-power terahertz radiation from relativistic electrons. *Nat.* **420**, 153.

Dua, H.W., Chena, M., Shenga, Z.M. & Zhanga, J. (2011). Numerical studies on terahertz radiation generated from two color laser pulse interaction with gas targets. *Laser Part. Beams* **29**, 447.

Faure, J., Tilborg, J.V., Kaindl, R.A. & Leemans, W.P. (2004). Single-shot spatiotemporal measurements of high-field terahertz pulses. *Opt. Quan. Electron.* **36**, 681.

Ferguson, B. & Zhang, X.C. (2002). Materials for terahertz science and technology. Nat. Mater. **1**, 26.

Garg, V. & Tripathi, V.K. (2010). Resonant third harmonic generation of an infrared laser in a semiconductor wave guide. *Laser Part. Beams* **28**, 327.

Ghorbanalilu, M. (2012). Second and third harmonics generations in the interaction of strongly magnetized dense plasma with an intense laser beam. *Laser Part. Beams* **30**, 291.

Giulietti, D., Banfi, G.P., Deha, I., Giulietti, A., Lucchesi, M., Nocera, L. & Zun, C.Z. (1988). Second harmonic generation in underdense plasma. *Laser Part. Beams* **6**, 141.

Hamster, H., Sullivan, A., Gordon, S., White, W. & Falcone, R.W. (1993). Subpicosecond, electromagnetic pulses from intense laser-plasma interaction. *Phys. Rev. Lett.* **71**, 2725.

Hamster, H., Sullivan, A., Gordon, S. & Falcone, R.W. (1994). Short-pulse terahertz radiation from high-intensity-laser-produced plasmas. *Phys. Rev. E* **49**, 671.

Hashimshony, D., Zigler, A. & Papadopoulos, K. (1999). Generation of tunable far-infrared radiation by the interaction of a superluminous ionizing front with an electrically biased photoconductor. *Appl. Phys. Lett.* **74**, 1669.

Houard, A., Liu, Y., Prade, B., Tikhonchuk, V.T. & Mysyrowicz, A. (2008). Strong Enhancement of terahertz radiation from laser filaments in air by a static electric field. *Phys. Rev. Lett.* **100**, 255006.

Hu, G.Y., Shen, B., Lei, A., Li, R. & Xu, Z. (2010). Transition Cherenkov radiation of terahertz generated by superluminous ionization front in femtosecond laser filament. *Laser Part. Beams* **28**, 399.

Jiang, Y., Li, D., Ding, Y.J. & Zotova, I.B. (2011). Terahertz generation based on parametric conversion from saturation of conversion efficiency to back conversion. *Opt. Lett.* **36**, 1608.

Kumar, K.K.M. & Tripathi, V.K. (2013). Third harmonic generation of a nonlinear laser Eigen mode of a self sustained plasma channel. *Laser Part. Beams* **31**, 163.

Ladouceur, H.D., Baronavski, A.P., Lohrmann, D., Grounds, P.W. & Girardi, P.G. (2001). Electrical conductivity of a

https://doi.org/10.1017/S026303461400024X Published online by Cambridge University Press

femtosecond laser generated plasma channel in air. *Opt. Commun*. **189**, 107.

Leemans, W.P., Tilborg, J.V., Faure, J., Geddes, C.G.R., Toth, C., Schroeder, C.B., Esarey, E., Fubioni, G. & Dugan, G. (2004). Terahertz radiation from laser accelerated electron bunches. *Phys. Plasmas* **11**, 2899.

Liu, C.S. & Tripathi, V.K. (2009). Tunable terahertz radiation from a tunnel ionized magnetized plasma cylinder. *J. Appl. Phys*. **105**, 013313.

Loffler, T., Kress, M., Thomson, M. & Roskos, H.G. (2005). Efficient Terahertz pulse generation in laser-induced gas plasmas. *Acta Phys.Polonica A* **107**, 1.

Loffler, T., Jacbo, F. & Roskos, H.G. (2000). Generation of terahertz pulses by photoionization of electrically biased air. *Appl. Phys. Lett*. **77**, 453.

Malik, A.K. & Malik, H.K. (2013). Tuning and focusing of terahertz radiation by dc magnetic field in a laser beating process. *IEEE J. Quant. Electron*.**49**, 232.

Malik, A.K., Malik, H.K. & Kawata, S. (2010). Investigations on THz radiation generated by two superposed femtosecond laser pulses. *J. Appl. Phys*. **107**, 113105.

Markelz, A., Roitberg, A. & Heilwiel, E. (2000). Pulsed terahertz spectroscopy of DNA, bovine serum albumin and collagen between 0.1 and 2.0 THz. *Chem. Phys. Lett*. **320**, 42.

Mittleman, D., Jacobsen, R. & Nuss, M. (1996). T-ray imaging. *Quan. Electron*. **2**, 679.

Panwar, A., Ryu, C.M. & Kumar, A. (2013). Effect of plasma channel non-uniformity on resonant third harmonic generation. *Laser Part. Beams* **31**, 531.

Paknezhad, A. & Dorranian, D. (2011). Nonlinear backward Raman Scattering in the short laser pulse interaction with a cold under dense transversely magnetized plasma. *Laser Part. Beams* **29**, 373.

Pickwell, E. & Wallace, V.P. (2006). Biomedical applications of terahertz technology. *J. Phys. D: Appl. Phys*. **39**, R301.

Pukhov, A. (2003). Strong field interaction of laser radiation. *Rep. Prog. Phys*. **66**, 47.

Sharma, R.P., Monika, M., Sharma, P., Chauhan, P. & Jia, A. (2010). Interaction of high power laser beam with magnetized plasma and THz generation. *Laser Part. Beams* **28**, 531.

Shen, Y.C., Today, T.Lo.P.F., Cole, B.E., Tribe, W.R. & Kemp, M.C. (2005). Detection and identification of explosives using terahertz pulsed spectroscopic imaging. *Appl. Phys. Lett*. **86**, 241116.

Shi, W., Ding, Y.J., Fernelius, N. & Vodopyanov, K. (2002). Efficient, tunable, and coherent 0.18–5.27-THz source based on GaSe crystal. Opt. Lett. **27**, 1454.

Tani, M., Gu, P., Hyodo, M., Sakai, K. & Hidaka, T. (2000). Generation of coherent terahertz radiation by photo mixing of dual-mode lasers. *Opt. Quan. Electron*. **32**, 503–520.

Tripathi, V.K. & Liu, C.S. (1990). Plasma effects in a free electron laser. *IEEE Trans. Plasma Sci*. **18**, 466.

Verma, U. & Sharma, A.K. (2009). Laser second harmonic generation in a rippled density plasma in the presence of azimuthal magnetic field. *Laser Part. Beams* **27**, 719.

Verma, U. & Sharma, A.K. (2011). Nonlinear electromagnetic Eigen modes of a self created magnetized plasma channel and its stimulated Raman scattering. *Laser Part. Beams* **29**, 471.

Varshney, P., Sajal, V., Singh, K.P., Kumar, R. & Sharma, N.K. (2013). Strong terahertz radiation generation by beating of extraordinary mode lasers in a rippled density magnetized plasma. *Laser Part. Beams* **31**, 337.

Walther, M., Fischer, B. & Schall, M. (2000). Far-infrared vibrational spectra of all-trans, 9-cis and 13-cis retinal measured by THz time-domain spectroscopy. *Chem. Phys. Lett*. **332**, 389.

Wang, T.J., Daigle, J.F., Yuan, S., Theberge, F., Chateauneuf, M., Dubois, J., Roy, G., Zeng, H. & Chin, S. L. (2011). Remote generation of high-energy terahertz pulses from two-color femtosecond laser filamentation in air. *Phys. Rev. A* **83**, 053801.

Zhao, P., Ragam, S., Ding, Y.J. & Zotova, I.B. (2010). Compact and portable terahertz source by mixing two frequencies generated simultaneously by a single solid-state laser. *Opt. Lett*. **35**, 3979.

Zheng, H., Redo-Sanchez, A. & Zhang, X.C. (2006). Identification and classification of chemicals using terahertz reflective spectroscopic focal-plane imaging system. *Opt. Express* **14**, 9130.

https://doi.org/10.1017/S026303461400024X Published online by Cambridge University Press